Characterization of Terahertz Beam Profile and Propagation

John F. Molloy, Mira Naftaly, and Richard A. Dudley

***Abstract*—Two techniques for imaging a terahertz (THz) beam profile are described and employed in characterizing the THz beam propagation in a time-domain spectrometer. Aperture scanning yields a 2-D cross-sectional map of field amplitude at selected frequencies that is used to track beam evolution along its path. The Hartmann test produces a 2-D topographical image of the wavefront, also at selected frequencies. The results are compared with theory, and the respective advantages of the two methods are discussed.**

***Index Terms*—Optical beams, physical optics, submillimeter wave imaging, submillimeter wave propagation.**

I. Introduction

THE recent rapid growth in terahertz (THz) measurements and applications has been made possible by the proliferation of time-domain spectrometers (THz TDS). Indeed, several manufacturers now offer flexible, compact, and affordable THz TDS systems (e.g., [1]–[3]). Despite this, relatively little work has been done on analyzing the optical properties and beam propagation in typical THz TDS configurations, unlike other commonly employed spectrometers such as grating monochromators and Fourier-transform interferometers. This may be attributed to the fact that the behavior of optical beams whose wavelength is much smaller than the dimensions of optical elements is well understood, and that visible and near-infrared beam profiles are easily examined using CCD cameras. Neither is the case for quasi-optical THz beams.

THz TDS systems are designed and aligned assuming perfect Gaussian beams [4]. However, deviations from the Gaussian profile may occur due to mirror imperfections, system misalignment, or emitter characteristics [5]. Variations from a plane surface present in the wavefront of the THz beam act to reduce the detected amplitude of the time-domain signal due to the spatial averaging of signal components undergoing different pulse evolution. Such averaging also causes an apparent broadening of the time-domain pulse, reducing the bandwidth of the calculated Fourier-transform frequency spectrum [4]. When the TDS is used for phase sensitive imaging, phase variations across the wavefront cause image degradation [6].

Furthermore, due to its broadband nature, THz TDS is mostly used for spectroscopy. The complex dielectric constants of materials studied are calculated from their transmitted spectra based on the assumption that all parts of the THz beam experience identical optical thickness and interact equally with the material [7]. If the THz wavefront is nonplanar, parts of the beam may travel through nonequivalent paths, leading to errors, especially in the refractive index [8]. The beam wavefront may also become further distorted by passage through the material, affecting the spatial and temporal signal-probe overlap at the detector, and causing frequency-dependent errors in the detected amplitude [9].

A detailed understanding of THz beam propagation through a TDS can aid system design and help improve system performance, for example, by increasing its bandwidth and lowering the noise floor, as well as by reducing uncertainties in the derived transmission parameters. Alongside modeling, a full experimental characterization of THz beams in a TDS is necessary in order to provide observational data and validate the model. This requires that both the temporal and spatial variations of the electrical field be measured at cardinal points along the beam path [10].

Whereas considerable effort, both theoretical and experimental, has been directed into analyzing the temporal evolution of THz pulses, studies into the spatial distribution of the *E*-field have been lacking [10]. A number of experimental factors account for this imbalance. In the first instance, THz TDS systems are generally configured to measure the field at only a single position, a focal point within the system, where the spatial distribution is small and the wavefront is assumed to be flat [11]. Moreover, the measurement of spatial beam distribution is inconvenient and time consuming.

Several methods have been developed for spatial imaging of THz beams. The simplest and least informative technique is to use a variable aperture placed within the beam and closed down in successive steps, recording a spectrum for each. The beam profile at selected frequencies is determined by plotting the Fourier transform derived amplitude against the iris diameter. Although simple and easy to perform, this approach suffers from two drawbacks. First, it provides only an area integral of the field amplitude across the beam, not a map of the wavefront. More importantly, it is liable to significant and unquantifiable error due to edge diffraction [12], [13].

A more advanced form of this method involves traversing a knife-edge mask through the beam while recording the resulting spectrum at multiple transverse points [13]–[15]. The amplitude

Manuscript received April 1, 2012; revised June 19, 2012; accepted June 20, 2012. Date of publication June 22, 2012; date of current version February 1, 2013. This work was supported by the National Measurement office of the U.K., and by the Engineering and Physical Sciences Research Council through the Industrial Doctoral Centre at Heriot-Watt University, Edinburgh, U.K.

The authors are with the National Physical Laboratory, Teddington, TW11 0LW, U.K. (email: john.molloy@npl.co.uk; mira.naftaly@npl.co.uk; richard.dudley@npl.co.uk).

Color versions of one or more of the figures in this paper are available online at http://ieeexplore.ieee.org.

Digital Object Identifier 10.1109/JSTQE.2012.2205668

at selected frequencies is then plotted against the transverse displacement, resulting in an approximately error-function curve, and the beam profile is derived by differentiating with respect to position. The knife-edge can be used to slice the beam along several directions, providing multiple profiles and revealing deviations from cylindrical symmetry.

More complex methods have also been used. Dickhoff *et al.* coupled THz radiation into a small polyethylene waveguide, connected to a power meter, which was raster-scanned through the beam [16]. Various types of detecting elements, such as electro-optic crystals [17] or GaAs dipole antennas with substrate lenses [18], [19] have been used as single-point detectors, scanned transversely through the beam in order to examine the effects of off-axis parabolic lenses [18], hyperhemispherical silicon lenses [18], [19], and free space propagation [17]. This method is made cumbersome by the necessity of realigning the laser beams for each measurement position so as to maintain the equidistance of pump and probe pulse travel [10]. In contrast, Zhang and coworkers obtained a 2-D record of the electrical field using an electro-optic crystal in conjunction with a CCD camera [20]–[22]. However, these measurements tend to suffer from small dynamic range and poor signal-to-noise ratio (SNR) [10]. In addition, the procurement of a suitably homogenous electro-optic crystal appears to be problematic. Bitzer *et al.* [10] used a gimbals mounted mirror to scan the THz beam across a standard THz-TDS setup in order to examine the effect of a plano-convex Teflon lens [10]. While this system avoids the previous issues, it requires significant room to operate.

These studies have mainly been conducted on THz TDS systems grossly resembling commonly implemented configurations, modified for the purpose of spatially resolving the electromagnetic field. They are generally capable of examining only a single optical element in the beam path, and are not readily adapted to use within pre-existing multielement systems.

We report on two simple techniques that allow the spatial distribution of the THz beam to be resolved in both the temporal and frequency domains: aperture scanning, and the Hartmann test. Both are readily applicable to pre-existing THz TDS systems, with no adjustment to the optical setup being necessary.

II. THz Beam Imaging Techniques

A. Aperture Scanning

To image the THz beam profile of a TDS, a large beam stop with a small aperture is placed in the beam path. The aperture samples the beam spatially at whichever point it is placed so that a complete coherent image of the beam profile at that axial position can be built up by raster-scanning the aperture transversely to the beam (see Fig. 1).

The beam stop containing the aperture must be sufficiently large to block the THz beam completely without allowing diffracted or scattered radiation to leak around its edges and reach the detector. The selection of the correct size of the aperture is of considerable importance. The long wavelength leads to strong beam divergence; hence, it is necessary to choose an aperture that will not cause a large fraction of the radiation to be diffracted out of the diameter of the collecting mirror. In addition, a compromise must be achieved between the competing needs for high spatial resolution, necessitating a small aperture, and acceptable SNR, requiring sufficiently large signal arriving at the detector.

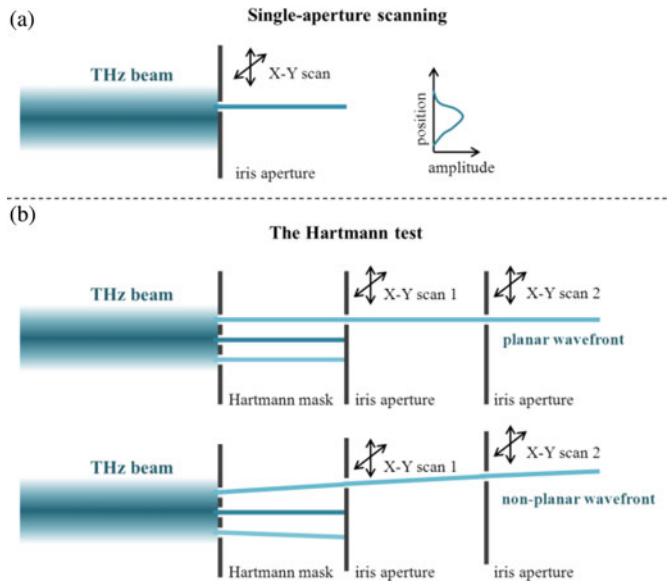

Fig. 1. Schematic depiction of (a) single-aperture scanning and (b) the Hartmann test.

The minimum aperture radius can be calculated by considering diffraction. For circular apertures, 0.84 of incident energy falls within the Airy disk [23], i.e., the first diffraction minimum. The aperture, therefore, should be such that the Airy disk is contained within the area of the collecting mirror. The location of the minima in a diffraction pattern [23] are given by

$$d \sin\theta_m = m\lambda \tag{1}$$

where d is the diameter of the aperture, λ is the wavelength, and m is an integer representing the diffraction order; for the Airy disk, $m = \pm 1$. In order for the Airy disk to fall within the area of the mirror, the angular displacement of the first diffraction order θ_1 must be such that $\sin\theta_1 \leq r/l$, where r is the radius of the collecting mirror, and l is the propagation distance. The minimum aperture is then

$$d \geq \frac{\lambda l}{r} \tag{2}$$

which is proportional to the wavelength. Since d varies across the THz band, a compromise value must be adopted.

Alternatively, the minimum aperture may be derived directly from the recorded THz spectrum, by assuming a minimum acceptable dynamic range. The aperture size is then determined experimentally as that which allows sufficient signal amplitude to be registered by the detector. It may be expected that the two aperture sizes arrived at using these different methods will be roughly similar.

B. Hartmann Test

The Hartmann test is an established technique measuring the profile of a wavefront, originally developed by J. Hartmann

(1900) [24], and used mostly to test for aberrations in the primary mirrors of telescopes. The test consists of placing a Hartmann mask or screen, which is an opaque screen perforated by an array of small holes, over the telescope's aperture. These holes allow pencil beams of light to be accepted into the optical system and imaged. If the incoming wavefront is flat and the lens is without aberrations, the beam array will be imaged to a point at the focus. Similarly, sampling the beams' paths inside and outside of the focus will produce two symmetric but magnified images of the array of holes. Should the hole images be connected by straight lines, it will be found that they all intersect at a common point, the paraxial focus [25]. If, however, the wavefront is not planar, then these beams will not all reach a common focus.

While aperture scanning reveals the frequency-dependent amplitude distribution across the THz beam, it does not detect the wavefront topography. In contrast, the Hartmann test determines the local angular inclination of the wavefront relative to the beam propagation axis, and thus maps out the phase profile of the wavefront. It is, therefore, more suited than aperture scanning to identifying beam distortions and especially to tracking beam evolution through the system.

In the present case a lens is not used to image the beams from the Hartmann mask. That is because the aim is to characterize an existing THz system without inserting additional optical elements, and also because lenses are generally problematic at THz frequencies. Instead, an aperture is scanned behind the mask at two locations so as to create an image of the pencil beams (see Fig. 1). The location of the centroid (center of mass) of each beam is then determined for both images. From this, knowing the separation between the two imaging planes, the angular deviation of the pencil beam from normal propagation can be calculated. This angular deviation can be related to the local aperture-averaged first derivative, i.e., the slope, of the wavefront at that point [26]. The wavefront can then be reconstructed as a series of intersecting planes.

Two key points must be considered in the design and operation of a Hartmann mask. First, it is desirable to maximize the resolution of the system, i.e., the smallest local tilt detectable, by minimizing the spot size of the pencil beams at the detection plane, without undue diffraction effects.

Second, consideration must be given to the size of the area sampled. In general, the area sampled by the detector for each aperture should be twice as large as the square of maximum displacement [24]. In astronomical applications, this is usually determined by theoretical models of a type not appropriate for the task at hand. Thus, we sample an area equal to the size of the mask, to avoid loss of spatial resolution when calculating the centroid of each beam. As the sampled beam is expected to be approximately collimated, the wavefront is assumed to be a plane surface convolved with a slowly varying function in X and Y directions [23].

The angular displacement of the two centroids relative to the beam axis ϕ is related to the transverse displacement at the measurement plane x by [23]

$$\phi = \tan^{-1} \frac{x}{L} \tag{3}$$

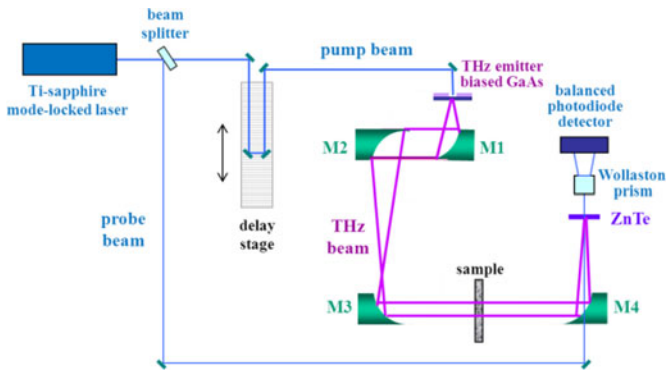

Fig. 2. Schematic drawing of the THz TDS used in beam imaging experiments.

where L is the distance along the Z-axis between the two images. The phase change g across the aperture of diameter D, i.e., the phase gradient is then related to the angular displacement by [26]

$$g = \frac{2\pi\phi D}{\lambda}. \tag{4}$$

The ideal scenario would be a mask containing a single aperture that could be scanned across the beam profile. This single aperture would then be imaged by a second scanned aperture, giving an almost unlimited spatial resolution of the wavefront. However, such an experiment would require prohibitively long imaging times, as well as necessitate the complications of employing two simultaneously scanning X–Y translation stages.

An alternative solution was, therefore, adopted, which avoided scanning of the first aperture by substituting a fixed array of apertures cut in a thin sheet of THz-opaque material. The array of beams produced by the Hartmann mask was then imaged at two distances along the beam path using single-aperture scanning as described earlier (see Fig. 1). Although the spatial resolution of this method is lower than that of double-aperture scanning, it is simpler and easier to implement.

The Hartmann mask was chosen to be a square array of circular apertures. A square array is the most suitable for imaging by raster scanning, while circular apertures avoid the spatial noise and asymmetric diffraction associated with corners. The diameter of each aperture was chosen to be equal to that used in single aperture scanning (see above). The spacing between aperture centers must be such as to provide clear discrimination between beam images, while maintaining good resolution. Allowing for diffraction, this can be achieved by setting the separation between aperture edges to be equal to aperture diameter, i.e., the distance between aperture centers is equal to twice their diameter.

III. Experimental Details

A. *THz Time-Domain Spectrometer*

The THz TDS used to demonstrate the beam imaging techniques is a commonly employed configuration shown in Fig. 2. The pump laser is a mode-locked Ti:Sapphire laser (Femtosource) with a 20-fs pulse length and a center wavelength of 800 nm, producing an average power of 450 mW.

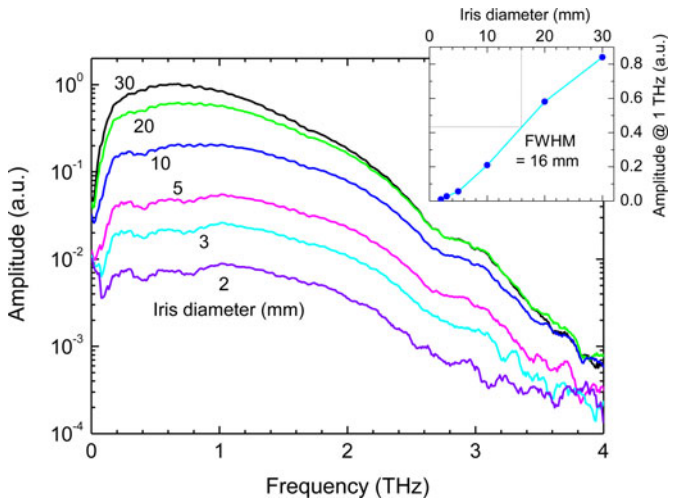

Fig. 3. THz spectra recorded with a variable aperture placed in the collimated beam between mirrors M3 and M4. Inset: amplitude at 1 THz versus iris diameter.

The THz source is a biased photoconductive emitter. The substrate is semiinsulating GaAs; the electrodes are formed by 300-μm thick silver dag, and are parallel with a gap of 1 mm. The emitter is mounted on copper blocks that form outer electrodes and facilitate cooling. The bias voltage is 200 V, with unipolar square-wave modulation at 10 kHz. THz signal is detected electro-optically, using a 1-mm thick ZnTe crystal. The maximum dynamic range of the system was $\sim$2000 in amplitude (at 0.6 THz, see Fig. 3).

The THz radiation is guided through the system by a set of four off-axis 90° parabolic mirrors, as shown in Fig. 2. All mirrors have the diameter of 75 mm. The effective focal length of mirrors M1 and M3 is 25 mm, and that of M2 and M4 is 75 mm. The nominal beam diameter of the collimated section of the beam between mirrors M3 and M4 is, therefore, 25 mm. The short focal length and large diameter of mirror M1 allow for a sufficiently large fraction of THz radiation to be collected from the emitter, dispensing with the need for a silicon hyperhemispherical lens. The focal point between mirrors M2 and M3 is used primarily for imaging, where objects may be raster-scanned through the beam focus. The 3:1 ratio in the focal lengths of M2 and M3 is designed to reduce the diameter of the collimated beam section between mirrors M3 and M4, which is employed for transmission spectroscopy. Using a collimated beam for spectroscopic measurements avoids errors arising from beam distortion that may be caused by placing a sample at the beam focus [8]. This nominally collimated beam section, which is 775 mm long, is also particularly suited for beam imaging using both single-aperture scanning and the Hartmann test.

B. Aperture Scanning

The longest free space propagation distance in the TDS system is the nominally collimated beam section between mirrors M3 and M4 that is 775 mm long, this can be used as the limiting case within the system. From (3), the minimum diameter of an aperture placed near M3 that will allow the Airy disk to fall within the area of M4 is 3.1 mm at 1 THz (300 μm) and 1.0 mm at 3 THz (100 μm).

To determine the minimum aperture that would maintain acceptable SNR, an adjustable iris was placed in the center of the beam between mirrors M3 and M4 (85 mm from M3). The diameter of the iris was reduced in steps, and a spectrum recorded for each (see Fig. 3). It was decided that SNR $\geq$ 10 at 1 THz is the minimum acceptable for adequate signal analysis. This corresponds to an iris diameter of $\sim$2 mm. However, this does not allow for the decrease in SNR at higher frequencies. An aperture of 3 mm was selected as a good compromise between acceptable SNR and sufficient spatial resolution. This will also ensure that the Airy disk for all frequencies above 1 THz will be contained within the area of mirror M4.

The aperture was a steel variable iris diaphragm mounted on a precision translation stage. The iris was raster-scanned across the THz beam, and a time-domain trace was recorded every 1.5 mm along both *X* and *Y* axes, producing an imaged area of 45 $\times$ 45 mm composed of 30 $\times$ 30 "pixels."

Using this configuration, the THz beam was then sampled at six locations along its path (listed as follows): at three points between mirrors M2 and M3, including at the focus; and at three points along the collimated section between mirrors M3 and M4. It was not possible to sample the THz beam between M4 and the electro-optic crystal, as the mask would have blocked the copropagating probe beam (see Fig. 2). Likewise, due to the close proximity of the emitter to mirror M1, and of mirror M1 to M2, it was not possible to image the beam in those locations.

C. Hartmann Test

The Hartmann mask was a 2-mm thick aluminum plate with circular apertures set on a square grid pattern. The diameter of each aperture was 3 mm, equal to that used for single aperture scanning. The distance between aperture centers was twice their diameter, i.e., 6 mm. The aperture grid was 8(H) $\times$ 9(V) holes and covered a rectangular area of 39(H) $\times$ 45(V) mm. A rectangle was chosen rather than a square because it was noted that the THz beam had a slightly oval cross section, with the horizontal extension being larger than the vertical. The Hartmann mask was positioned between mirrors M3 and M4, 85 mm from M3, at a point where a single-aperture scan had also been obtained.

The THz beam is nominally collimated between mirrors M3 and M4. Therefore deviations from a planar wavefront are expected to be small, of the order of 1°. The two imaging planes must be separated by sufficient distance to allow these angles to be measured with sufficient accuracy. Using the centroid, the centers of the aperture beams can be located with a spatial resolution of 0.1 aperture diameter (0.15 mm). In order to resolve an angular deviation of 3°, the distance between the imaging planes must be larger than 0.15/tan1° = 8.5 mm; for 0.7°, it is 12 mm. The distance chosen was therefore $\sim$12 mm. Similarly to single-aperture scanning, an area of 45 $\times$ 45 mm was imaged, composed of 30 $\times$ 30 "pixels".

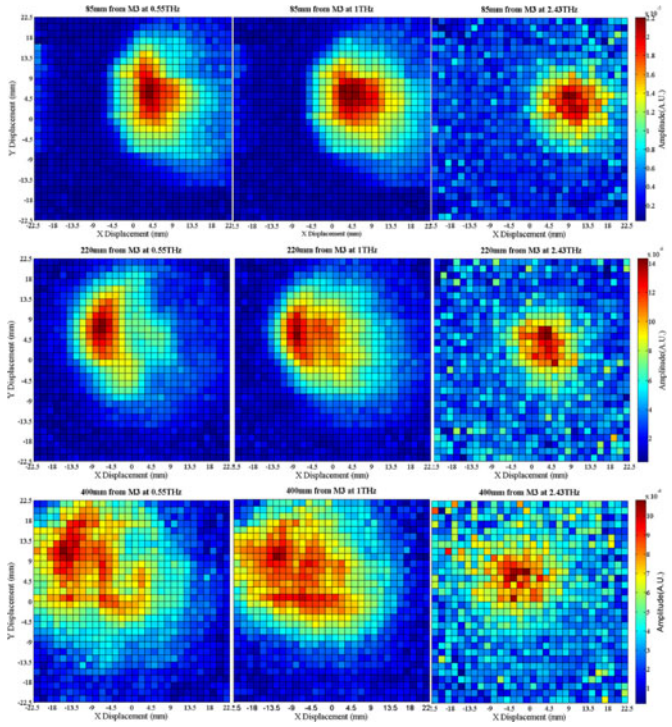

Fig. 4. THz beam profiles imaged using frequency-resolved aperture scanning, depicting beam evolution through the nominally collimated section between mirrors M3 and M4. Images obtained at three positions: 85, 220, and 400 mm from M3. Frequencies shown: 0.55, 1.0, and 2.45 THz.

IV. Results and Discussion

Aperture scanning was used to image the beam profile at three positions along the nominally collimated section between mirrors M3 and M4: at 85, 220, and 400 mm from M3. Fig. 4 shows the evolution of the beam at three frequencies: 0.55, 1.0 and 2.45 THz. The highest frequency suffers from low SNR due to its low amplitude. It is seen that the beam profile is distorted, and that different frequencies exhibit different distortion patterns. In particular, the collimation is imperfect. As expected, the lowest frequency shows the strongest divergence and largest beam diameter. Notably, all frequencies show significant asymmetry and irregularities in the beam profile. Given the small spatial extent of these variations, they may be attributed to imperfections in the mirrors rather than to gross misalignment.

The spatial variations in the beam intensity profile can be visualised more readily by plotting a 3-D map of the maximum of the time-domain peak, as shown in Fig. 5. Two notable deviations from the Gaussian form are evident. First, the profile is skewed, with a larger vertical extension than horizontal. This may be caused by the asymmetric radiation pattern from the THz emitter, whose electrodes are aligned vertically. Second, there are small localized irregularities, in particular, a distinct dip at half-height. On examining the optics, the dip was found to be caused by a defect in the coating of mirror M2, as seen in Fig. 6.

It is worth comparing the information provided by Figs. 5 and 6 with that given by the inset in Fig. 3 that plots the amplitude at 1 THz versus iris diameter, as in [12]. This plot shows a smooth

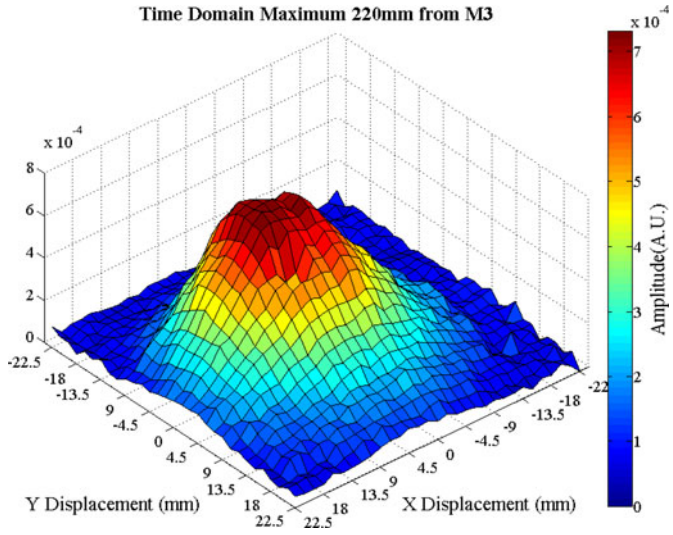

Fig. 5. THz beam profile imaged using aperture scanning, obtained by plotting the maximum of the time-domain peak. The image obtained 220 mm from M3.

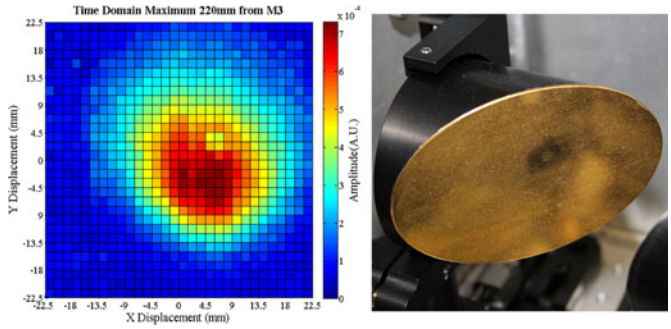

Fig. 6. THz beam profile as in Fig.5. (a) 2-D plot of field amplitude, showing an area of reduced amplitude (at $x = 6$; $y = 3$). b) Photograph of M2, where a defect in the coating can be seen at a location corresponding to the amplitude dip in the beam profile.

curve of integrated intensity, revealing none of beam distortions, asymmetries, or irregularities.

The THz beam was also imaged at three locations between mirrors M2 and M3, using aperture scanning: in the focal plane (150 mm from M2), 28 mm before the focus (122 mm from M2), and 10 mm after the focus (160 mm from M2). Fig. 7 depicts the frequency-resolved images obtained in the focal plane for 0.55, 1, and 2.45 THz. At the focus the beam diameter is too small to be resolved; nevertheless, it is clearly seen that the waist decreases at higher frequencies.

The expected THz beam diameter as it evolves through the focus can be calculated from the basic formulae of Gaussian beam propagation. The beam waist is given by [27]

$$w_0 \cong \frac{2\lambda f}{\pi D} \tag{5}$$

where D is the diameter of the aperture, in this case M2 so that $f/D = 2$. Away from the focus, the beam radius can be calculated from [27]:

$$w(z)^2 = w_0^2 \left[1 + \left(\frac{\lambda z}{\pi w_0^2}\right)^2\right] \cong \left(\frac{\lambda}{\pi w_0}\right) z = \frac{z}{4} \tag{6}$$

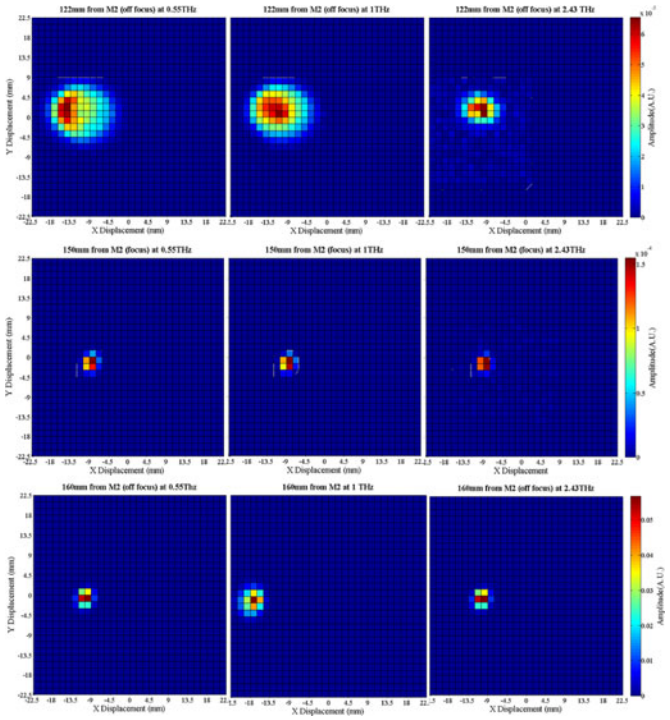

Fig. 7. THz beam profiles imaged using frequency-resolved aperture scanning, depicting beam evolution through the focus between mirrors M2 and M3. Images obtained at three positions: 122, 150 (focus), and 400 mm from M2. Frequencies shown: 0.55, 1.0, and 2.45 THz.

TABLE I
BEAM DIAMETERS, CALCULATED, AND MEASURED

Position From M2	Calculated FWHM (mm)					
	$\lambda = 545$ μm		$\lambda = 300$ μm		$\lambda = 125$ μm	
122 mm	11.7		11.7		11.7	
150 mm	1.2		0.6		0.3	
160 mm	4.2		4.2		4.2	
	Measured FWHM (mm) ±1.5 mm					
	$\lambda = 545$ μm		$\lambda = 300$ μm		$\lambda = 125$ μm	
	X	Y	X	Y	X	Y
122 mm	13.5	12.0	12.0	13.5	9.0	9.0
150 mm	<3.0	<3.0	<3.0	<3.0	<3.0	<3.0
160 mm	4.5	4.5	6.0	6.0	4.5	4.5

X – horizontal; Y – vertical.

where z is the distance from the focus. The expected values of THz beam diameter at the three imaging points are listed in Table I, together with the values obtained from the beam profile images shown in Fig. 7.

At the focus the beam diameter is below resolution, but away from the focus it conforms to the expected values, within uncertainty. The spot size of 2.45 THz at 122 mm appears to be smaller than expected due to the low amplitude and SNR at that frequency. It is notable that the profile of 0.55 THz at 122 mm shows significant distortion, consistent with that observed in the collimated beam section as seen in Fig. 4.

The Hartmann test produced a frequency-resolved topographical map of the beam wavefront, depicted in Fig. 8 for 1 THz. The mask was placed in the collimated section of the beam, 85 mm from M3, where aperture scanning had also been performed. The two scanning positions were 0.5 and 13.0 mm from the mask, respectively. The local inclination of the wavefront is indicated in Fig. 8 by arrows, where the arrow directions indicate inclination and their length is proportional to the angular deviation from planar.

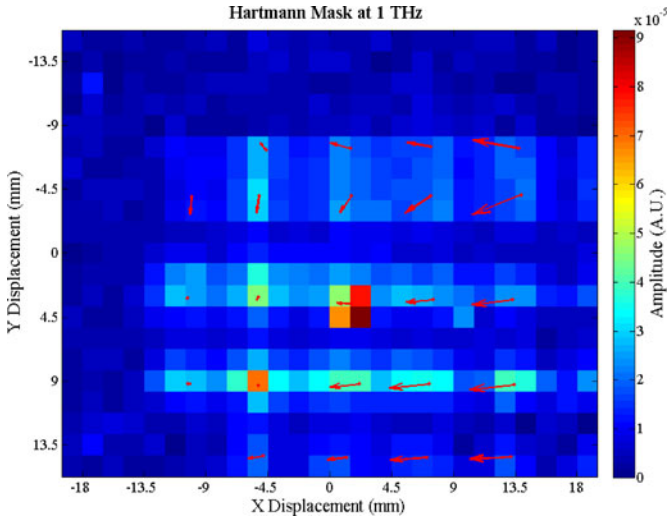

Fig. 8. Topographical map of the beam profile at 1 THz produced by the Hartmann test. Mask placed 85 mm from M2; scanning positions 0.5 and 13 mm from the mask. Arrow directions indicate wavefront inclination; arrow lengths are proportional to the angle from planar.

It is seen that in the wings of the beam the inclination tends to be greatest, as expected. The assymetries in the beam and the local variations are also clearly revealed. Notably, the inclinations in the horizontal direction are larger than in the vertical, which is consistent with the skewed beam profile seen in Fig. 5.

V. FAULT MITIGATION

Having observed the distortions and irregularities in the THz beam as shown in Figs. 4–7, it was decided to attempt improvements to the beam profile. To this purpose a new set of parabolic mirrors was purchased and inserted into the TDS. This resulted in dramatic improvements, as seen in Fig. 9(a).

The new beam is closer to Gaussian (compare with Fig. 6). The profile is more circularly symmetric, especially the central part. The wings, however, still exhibit significant asymmetry, and the peak maximum is displaced off-center. Nevertheless, unlike in Fig. 6, the profile has a single, localized, well-defined maximum. The local irregularities have also been removed, and the dip in the center has disappeared. The beam diameter has been reduced to approximately 26 mm (2σ), which is close to the expected value of 25 mm, indicating improved beam collimation.

In addition, the measured THz spectrum exhibited significantly increased SNR at frequencies above 1.5 THz [see Fig. 9(b)]. This may be attributed to two factors. First, reduced beam distortion and improved copropagation of frequency components, resulting in increased signal-probe overlap at all frequencies. And second, reduced reflection losses at higher frequencies, due to better mirror quality.

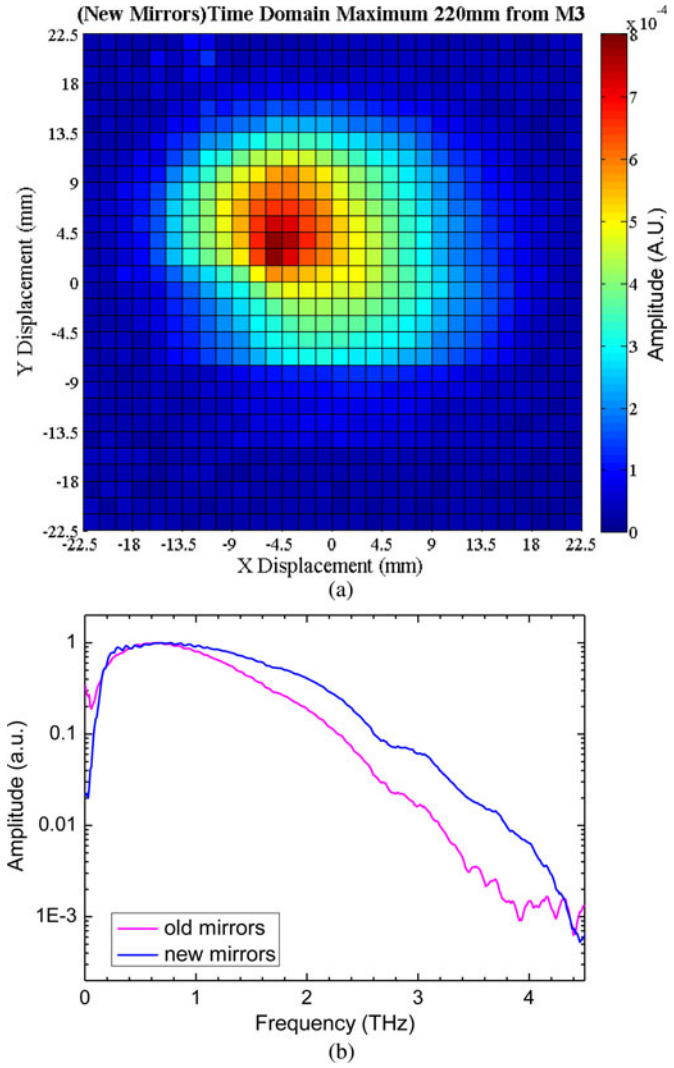

Fig. 9. (a) THz beam profile 220 mm from M3, obtained using aperture scanning, as in Fig. 5. (b) THz spectrum produced with the old and new set of parabolic mirrors in the TDS system.

These results demonstrate the utility of beam imaging in detecting and rectifying flaws in beam propagation, leading to improvements in system performance.

VI. Conclusion

We have described two techniques for imaging the profile of a THz beam and have demonstrated their application on a standard TDS. Both techniques produce a 2-D map of the beam profile are convenient and easy to apply and do not require a reconfiguration of the optical system. Aperture scanning maps the frequency resolved amplitude of the THz field at the scanning positions, and can be used to visualize the evolution of the beam intensity distribution through the optical system. Each map reveals both the gross profile of the beam and localized irregularities, its spatial resolution being limited by the size of the aperture.

The Hartmann test produces a frequency-resolved topographical map of the beam wavefront, revealing deviations from the planar wave. In principle, the Hartmann test applied at a single location may allow to calculate the evolution of the beam through the entire optical system. In the present case, the test was designed to detect small deviations in a slowly varying wavefront. For a more distorted beam, where larger wavefront slopes are expected, the mask separation would be reduced to increase the maximum measurable slope.

Measurements on a TDS revealed significant deviations from the ideal Gaussian profile that were clearly depicted and identified. While a grossly skewed beam shape may be observable using a knife-edge test, small-scale irregularities would not be detected. In particular, a local defect in a mirror coating was seen to produce a corresponding dip in the amplitude map of the beam. Replacing the parabolic mirrors and realigning the system resulted in clearly observed improvements in the beam profile and increased SNR at higher frequencies, validating the technique and confirming its utility.

References

[1] Picometrix. (2012). [online]. Available: http://www.picometrix.com/.
[2] Teraview. (2012). [online]. Available: http://www.teraview.com/.
[3] Zomega. (2012). [online]. Available: http://www.zomega-terahertz.com/.
[4] Y.-S. Lee, *Principles of Terahertz Science and Technology*. Berlin, Germany: Springer, 2009.
[5] P. Kužel, M. A. Khazan, and J. Kroupa, "Spatiotemporal transformations of ultrashort terahertz pulses," *J. Opt. Soc. Amer. B*, vol. 16, pp. 1795–1800, 1999.
[6] D. Mittleman, "Terahertz imaging," in *Sensing With Terahertz Radiation*, D. Mittleman, Ed. Berlin, Germany: Springer, 2003, ch. 2.
[7] D. Grischkowsky, S. Keiding, M. van Exter, and C. Fattinger, "Far-infrared time-domain spectroscopy with terahertz beams of dielectrics and semiconductors," *J. Opt. Soc. Amer. B*, vol. 7, pp. 2006–2015, 1990.
[8] J. W. Bowen, G. C. Walker, S. Hadjiloucas, and E. Berry, "The consequences of diffractively spreading beams in ultrafast terahertz spectroscopy," in *Proc. Joint 29th Int. Conf. Infrared Millimeter Waves 12th Int. Conf. Terahertz Electron.*, 2004, pp. 551–552.
[9] F. Théberge, M. Châteauneuf, and J. Dubois, "Effects of spatial coherence distortion on terahertz time-domain spectroscopy," *Appl. Phys. Lett.*, vol. 92, no. 18, pp. 183501-1–183501-3, 2008.
[10] A. Bitzer, M. Walther, A. Kern, S. Gorenflo, and H. Helm, "Examination of the spatial and temporal field distributions of single-cycle terahertz pulses at a beam focus," *Appl. Phys. Lett.*, vol. 90, pp. 071112-1–0711121-3, 2007.
[11] W. Withayachum, B. M. Fischer, and D. Abbott, "Material thickness optimization for transmission-mode terahertz time-domain spectroscopy," *Opt. Express*, vol. 16, pp. 7382–7396, 2008.
[12] A. Podzorov, A. Wojdyla, and G. Gallot, "Beam waist measurement for terahertz time-domain spectroscopy experiments," *Opt. Lett.*, vol. 35, pp. 901–903, 2010.
[13] Y. Wang, Z. Zhao, Z. Chen, L. Zhang, and K. Kang, "Analysis of terahertz pulse propagation through a dielectric edge," *Proc. SPIE*, vol. 7277, pp. 72770R-1–72770R-8, 2009.
[14] H Lin, C. Fumeaux, B. M. Fischer, and D. Abbott, "Modelling of subwavelength THz sources as Gaussian apertures," *Opt. Express*, vol. 18, pp. 17672–17683, 2010.
[15] A. Dobroiu, M. Yamashita, Y. N. Ohshima, Y. Morita, C. Otani, and K. Kawase, "Terahertz imaging system based on a backward-wave oscillator," *Appl. Opt.*, vol. 43, pp. 5637–5646, 2004.
[16] R. Dickhoff, C. Jastrow, A. Steiger, R. Müller, T. Keline-Ostmann, and T. Schrader, "Characterization of THz Beams," in *Proc. Quantum Electron. Laser Sci. Conf.*, OSA Technical Digest (CD) (Optical Society of America, 2011), paper JThB116.
[17] A. Gürtler, C. Winnewisser, H. Helm, and P. Uhd Jensen, "Terahertz pulse propagation in the near field and the far field," *J. Opt. Soc. Amer. A*, vol. 17, pp. 74–83, 2000.
[18] P. Uhd Jepsen, R. H. Jacobsen, and S. R. Keidling, "Generation and detection of terahertz pulses from biased semiconductor antennas," *J. Opt. Soc. Amer. B*, vol. 13, pp. 2424–2436, 1996.

[19] A. Bitzer, H. Hel, and M. Walther, "Beam-profiling and wavefront-sensing of THz pulses at the focus of a substrate-Lens," *IEEE J. Select. Topics Quantum Electron.*, vol. 14, pp. 476–480, 2008.
[20] Q. Wu, T. D. Hewitt, and X. C. Zhang, "Two-dimensional electro-optic imaging of THz beams," *Appl. Phys. Lett.*, vol. 69, pp. 1026–1028, 1996.
[21] Z. P. Jiang and X. C. Zhang, "2D measurement and spatio-temporal coupling of few-cycle THz pulses," *Opt. Express*, vol. 5, pp. 243–248, 1999.
[22] Z. P. Jiang and X. C. Zhang, "Terahertz imaging via electro-optic effect," *IEEE Trans. Microwave Theory Tech.*, vol. 47, pp. 2644–2650, 2000.
[23] E. Hecht, *Optics*. Reading, MA: Addison-Wesley, 2002, ch. 4.
[24] J. W. Hardy, *Adaptive Optics for Astronomical Telescopes*. London, U.K.: Oxford Univ. Press, 1998, ch. 5.
[25] J. M. Geary, "Wavefront sensors," in *Adaptive Optics Engineering Handbook*, R. K. Tyson and B. J. Thompson, Eds. New York: Marcel Dekker, 2000, ch. 6.
[26] Parenti, "System design and optimization," in *Adaptive Optics Engineering Handbook*, R. K. Tyson and B. J. Thompson, Eds. New York: Marcel Dekker, 2000, ch. 8.
[27] H. Kogelnik and T. Li, "Laser beams and resonators," *Appl. Opt.*, vol. 5, pp. 1550–1567, 1966.

John F. Molloy received the B.Sc degree in physics and astronomy from the National University of Ireland, Galway, Ireland, in 2006, and the M.Sc degree in photonics and optoelectronic devices jointly from the University of St. Andrews, St. Andrew, U.K., and Heriot Watt University, Edinburgh, U.K, in 2011. He is currently working toward the Eng. D. degree at Heriot-Watt University, Edinburgh, U.K.

Since 2011, he has been a Student with the National Physical Laboratory, Teddington, U.K., where his current research project focuses on the development of new tunable THz sources. Previously, he was with industry as a Laser Engineer supplying diode-pumped solid-state lasers, and as an Electronic Engineer developing high speed, high capacity storage solutions for digital media.

Mira Naftaly received the B.Sc. and M.Sc. degrees in physics from Technion—Israel Institute of Technology, Haifa, Israel, and the Ph.D. degree in physics from Brunel University, Middlesex, U.K., in 1989.

She is a Laser Physicist who has worked in the areas of spectroscopy and materials science. In 2002, she was with the Terahertz (THz) group at Leeds University, Leeds, U.K., where she focused on the THz area. Her main research interests in Leeds University included measurement system development and THz spectroscopy of materials including glasses, polymers, ceramics, and oils. Since 2008, she has been with National Physical Laboratory, where she involved in developing calibration methods for THz systems, with a focus on linearity frequency. She also continued research in materials spectroscopy, including ceramics, gases, and aqueous solutions of biomolecules.

Richard A. Dudley received the B.Sc. and Ph.D. degrees in applied physics from the University of Essex, Essex, U.K., in 1992 and 1996, respectively.

He joined the National Physical Laboratory (NPL) in 1996 to complement NPLs work on electro-optic sampling of high-speed electrical signals, later moving into the measurement of microwave-integrated circuit MMIC and on-wafer probing using network analysis to 110 GHz and free-space electric field measurement. He next assumed responsibility for the development and marketing of an NPL free-space electric-field measurement sensor, the optically modulated scattered (OMS), developing further interest in antenna and electric-field measurement systems. In 2005, he instigated the NPL terahertz activities and has developed measurement systems and calibration services for the frequency band 100 GHz–4 THz. More recently, he has been working on proposals for the calibration of microwave radiometer satellite payloads, for the accurate measurement of the Earth near-surface temperature from space.